Angular plasmon response of gold nanoparticles arrays: approaching the Rayleigh limit

Joseph Marae-Djouda, Roberto Caputo, Nabil Mahi, Gaëtan Lévêque,
Abdellatif Akjouj, Pierre-Michel Adam, Thomas Maurer

HAL Id: hal-02292656
https://utt.hal.science/hal-02292656

Research article   **Open Access**

Joseph Marae-Djouda, Roberto Caputo*, Nabil Mahi, Gaëtan Lévêque, Abdellatif Akjouj, Pierre-Michel Adam and Thomas Maurer

Angular plasmon response of gold nanoparticles arrays: approaching the Rayleigh limit

Abstract: The regular arrangement of metal nanoparticles influences their plasmonic behavior. It has been previously demonstrated that the coupling between diffracted waves and plasmon modes can give rise to extremely narrow plasmon resonances. This is the case when the single-particle localized surface plasmon resonance (λ_{LSP}) is very close in value to the Rayleigh anomaly wavelength (λ_{RA}) of the nanoparticles array. In this paper, we performed angle-resolved extinction measurements on a 2D array of gold nano-cylinders designed to fulfil the condition $\lambda_{\mathrm{RA}} < \lambda_{\mathrm{LSP}}$. Varying the angle of excitation offers a unique possibility to finely modify the value of λ_{RA}, thus gradually approaching the condition of coupling between diffracted waves and plasmon modes. The experimental observation of a collective dipolar resonance has been interpreted by exploiting a simplified model based on the coupling of evanescent diffracted waves with plasmon modes. Among other plasmon modes, the measurement technique has also evidenced and allowed the study of a vertical plasmon mode, only visible in TM polarization at off-normal excitation incidence. The results of numerical simulations, based on the periodic Green's tensor formalism, match well with the experimental transmission spectra and show fine details that could go unnoticed by considering only experimental data.

1 Introduction

Diffraction is the core working principle of a large amount of photonic devices and represents a remarkable effect of light-matter interaction. The speed of light in a medium depends on its refractive index; as such, a plane wave impinging on a medium whose refractive index is periodically modulated undergoes a wavefront distortion. For instance, light propagating through a phase diffraction grating results into a far-field light pattern made of areas illuminated at specific angles. The Fourier space representation of this phenomenon is reported in Figure 1. The vector equation governing the diffraction into a specific order m can be written as

$$\boldsymbol{k}_i + m\boldsymbol{q} = \boldsymbol{k}_d + \boldsymbol{\Delta}, \qquad (1)$$

where $k_i = n_{\mathrm{inc}} 2\pi/\lambda$ and $k_d = n_{\mathrm{dif}} 2\pi/\lambda$, respectively, are the moduli of the wave vectors of the light impinging on the grating and diffracted by it; $q = 2\pi/\Lambda$ is the modulus of the vector associated with the grating and Λ its period; n_{inc} and n_{dif} are respectively the refractive indices of the media where the light is coming from (before diffraction) and propagating to (after diffraction). Finally, the vector Δ is usually indicated as wave-mismatch and distinguishes the case of Bragg-matched ($\Delta = 0$; Figure 1A) and mismatched ($\Delta \neq 0$; Figure 1B) incidence [1].

*Corresponding author: Roberto Caputo, Laboratoire de Nanotechnologie et d'Instrumentation Optique, ICD CNRS UMR no. 6281, Université de Technologie de Troyes, CS 42060, 10004 Troyes, France, e-mail: roberto.caputo@fis.unical.it; and Physics Department, University of Calabria, 87036 Rende (CS), Italy
Joseph Marae-Djouda: Laboratoire de Nanotechnologie et d'Instrumentation Optique, ICD CNRS UMR no. 6281, Université de Technologie de Troyes, CS 42060, 10004 Troyes, France; and Ermess, EPF-Ecole d'ingénieurs, 3 bis rue Lakanal 92 330 Sceaux, France
Nabil Mahi: Institut d'Electronique, de Microélectronique et de Nanotechnologie (IEMN), CNRS-8520, Cité Scientifique, Avenue Poincaré, 59652 Villeneuve d'Ascq, France; and Laboratoire de Physique Théorique, Université Abou Bekr Belkaid – Tlemcen, B.P. 230 Tlemcen, Algeria
Gaëtan Lévêque and Abdellatif Akjouj: Institut d'Electronique, de Microélectronique et de Nanotechnologie (IEMN), CNRS-8520, Cité Scientifique, Avenue Poincaré, 59652 Villeneuve d'Ascq, France
Pierre-Michel Adam and Thomas Maurer: Laboratoire de Nanotechnologie et d'Instrumentation Optique, ICD CNRS UMR no. 6281, Université de Technologie de Troyes, CS 42060, 10004 Troyes, France
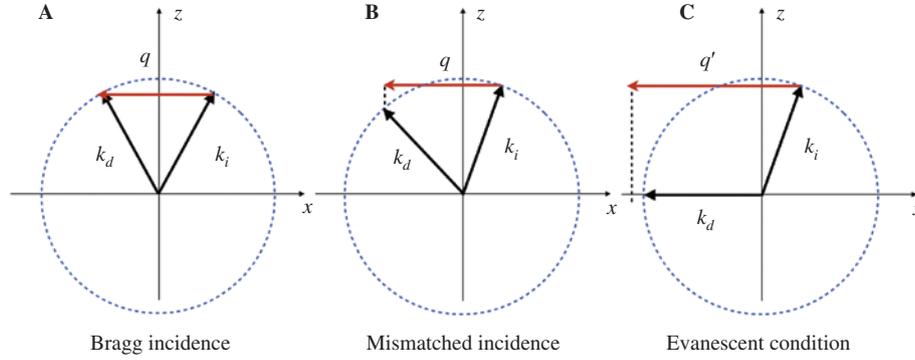
Figure 1: Typical Fourier space geometries in phase diffraction gratings. (A) Bragg incidence, (B) Bragg-mismatched incidence, and (C) evanescent (nonradiative) condition of a diffracted order.

In Figure 1C, the case when diffraction results in non-radiative or evanescent orders is instead depicted. This happens when

$$|mq| \geq k_{i,x} + k_d. \tag{2}$$

In the previous equation, the equality sign corresponds to the cut-off between radiative and evanescent diffracted orders. This limit has been first identified by Wood [2] and then explained by Rayleigh [3]. For this reason, Eq. (2) (with equality sign) is indicated as Rayleigh anomaly and commonly written as

$$m\lambda_{RA} = \Lambda(n_{inc}\sin\theta_{inc} + n_{dif}). \tag{3}$$

Noteworthy, the Rayleigh wavelength λ_{RA} depends on n_{inc}, n_{dif}, the angle θ_{inc}, formed by the beam incoming on the grating with its normal, and the considered diffracted order (m). Once previous parameters are fixed, the grating behaves in subwavelength (SW) regime for all wavelength values $\lambda > \lambda_{RA}$.

The behavior of the grating is peculiar when the diffracted order is evanescent. If the first order (m=+1) is considered, the electric field, associated with the diffracted wave, remains confined in proximity of the grating interface (with air, in this case) and can be written as

$$E_{dif} = A\exp(i\omega t)\exp(-ik\alpha x)\exp(-k\beta|z|), \tag{4}$$

which is the expression of a progressive wave propagating in the direction parallel to the grating (along x) with an amplitude term exponentially decaying in the direction orthogonal to the grating (along z) [4]. In the previous equation, $k = (2\pi/\lambda)n_{dif}$, while

$$\begin{cases} \alpha = \sin\theta_{dif} = \left|\dfrac{1}{n_{dif}}\left(\dfrac{m\lambda}{\Lambda} - \sin\theta_{inc}\right)\right| > 1 \\ \beta = \sqrt{\alpha^2 - 1} = \sqrt{\left[\dfrac{1}{n_{dif}}\left(\dfrac{m\lambda}{\Lambda} - \sin\theta_{inc}\right)\right]^2 - 1} \end{cases}. \tag{5}$$

θ_{dif} is the angle made by the considered diffracted beam with the grating normal. When the condition in Eq. (2) is verified for a specific diffracted order, the grating behaves in SW regime [5]. Many applications of SW gratings made of dielectric materials are reported in the literature. Even if made of isotropic materials, these gratings show a form of birefringence, thus an anisotropic response when illuminated by light of different polarization. This property has been exploited in several applications and mainly as antireflection layers [6], waveplates [7], for polarization control [8], and metamaterials [9]. Different is the situation when a grating is made of metallic stripes or arrays of metal nanoparticles (NPs). Actually, the lineshape features of the localized surface plasmon resonance (LSPR) of a single plasmon subunit are strongly influenced by the regular arrangement of the subunits. As suggested by Eq. (4), if the NP array is illuminated with a wavelength close to λ_{RA}, the considered diffracted order is evanescent and propagates along the sample substrate. The evanescent electric field associated with this order is localized in the substrate and can couple with the plasmon fields scattered by the particles, thus inducing a collective resonance (CR) mode [10]. Indeed, theoretical studies have demonstrated that this near-field coupling is much more efficient when the LSPR wavelength of the isolated metal NP (λ_{LSP}) is close in value to the Rayleigh wavelength ($\lambda_{LSP} \sim \lambda_{RA}$) [11–13]. This choice is functional to maximize the energy transfer between the evanescent waves, propagating in proximity of the substrate, and the NP plasmon modes. The evident consequence of this energy transfer is the modification and extreme narrowing of the LSPR lineshape. Schatz et al. [11, 12] have first suggested that these narrow resonances are possible in regular arrays of NPs, while Markel has elaborated the theory [13]. Several experimental verifications have also been provided [14–23], and considering the very narrow linewidth achievable (few nanometers), results hold promises for many applications in lasing, sensing, and metamaterials [24].

An interesting possibility is to study the coupling between diffractive and plasmon modes in the condition $\lambda_{RA} < \lambda_{LSP}$. In this paper, a short-pitch 2D array of Au nano-cylinders (designed and fabricated to the scope) produces purely evanescent orders for impinging wavelengths in the close vicinity of λ_{LSP}. The plasmonic properties of the array have been experimentally characterized by performing angular resolved extinction measurements. Depending on the incidence angle and polarization of the exciting light, it is possible to continuously follow the evolution of a grating-induced plasmon mode and the appearance of higher-order modes, including a vertical mode. Numerical simulations, performed on both isolated particles and arrays, allow the complete analysis of spectral position and origin of these modes.

2 Experiments

A 2D array of gold monomers (50×50 μm^2) was deposited by electron beam lithography on an indium tin oxide (ITO)-coated (30 nm thick) glass. The array consists of nano-cylinders (200 nm diameter, 50 nm height) with a (center-to-center) pitch $\Lambda_x = \Lambda_y = 300$ nm. Figure 2A shows a SEM picture of the fabricated sample.

A confocal transmission set-up, with angle-resolved measurement possibility, was used for the optical characterization of the sample. An illumination part, a multi-axis sample holder, and a collection part compose the set-up. All the parts are mounted on a rotating stage to allow maximum flexibility during measurements (Figure 2B). The UV-VIS-NIR light from the source lamp (tungsten) is brought to the illumination part by an optical fiber. This light is first polarized and then focussed, by a microscope objective ($20\times$, 0.28 NA), on the sample surface. The sample is fixed on the sample holder and can undergo a full (2π) rotation around an axis perpendicular to the optical table. Another microscope objective ($50\times$, 0.42 NA) collects the light transmitted by the sample. The diameters of illuminated and collection areas are respectively 300 μm and 10 μm. An analyser, put after this objective, is used to select the polarization of the transmitted light. A beam splitter sends 92% of this light to the spectrometer while the remaining amount goes to the camera and allows visualizing the area of the grating that is actually investigated. While performing angle-resolved extinction measurements, the sample holder was progressively turned, thus modifying the direction of the wave-vector impinging on the nano-cylinder array. For each measurement, the incidence angle was equal to the collection one and, for all angles, both longitudinal (TE) and transverse (TM) polarizations were considered according to the geometries depicted in Figure 3A and B.

The experimental extinction spectra measured at different angles in air (0°, 15°, 25°, 35°, 52°, and 60°), in TE and TM polarizations, are reported in Figure 4. With TE polarized light impinging on the sample at normal incidence, only one mode [$\lambda \sim 740$ nm, (1) in Figure 4A] is excited. The shape and spectral position of this mode suggest that the excitation of the incident light results in a dipolar mode with free-electrons oscillating along the diameter of the gold nano-cylinders [25, 26]. However, the quite visible red-shift of this mode, observed for both TE and TM polarizations at an increase of the incidence angle of the exciting light (Figure 4A and B), excludes that this is a purely dipolar mode as observed in case of a single NP: we expect that the regular arrangement of nano-cylinders influences their plasmonic behavior [27–29].
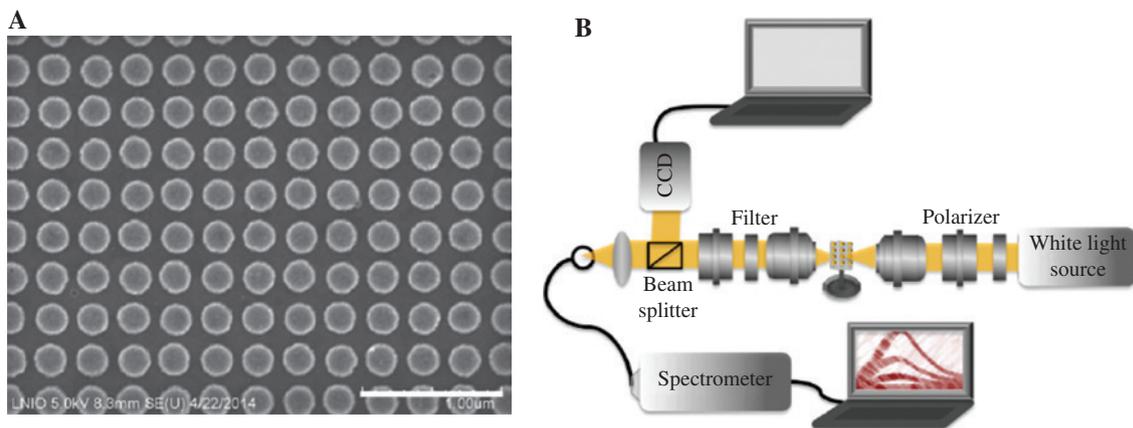

Figure 2: (A) SEM image of the grating of, gold nano-cylinders; the scale bar is 1 μm. The experimental set-up for angle-resolved extinction measurements is presented in (B).
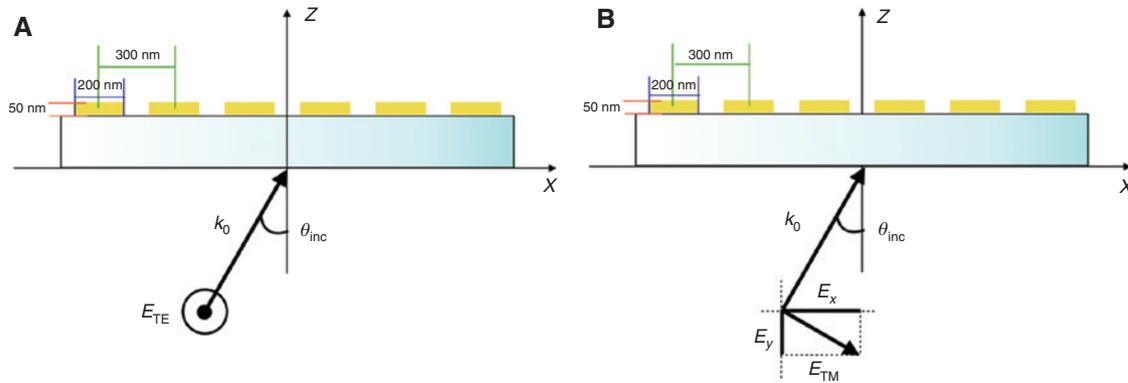
Figure 3: Geometrical configurations utilized during the angle-resolved extinction measurements, in case of TE (A) and TM (B) polarization of the exciting light.
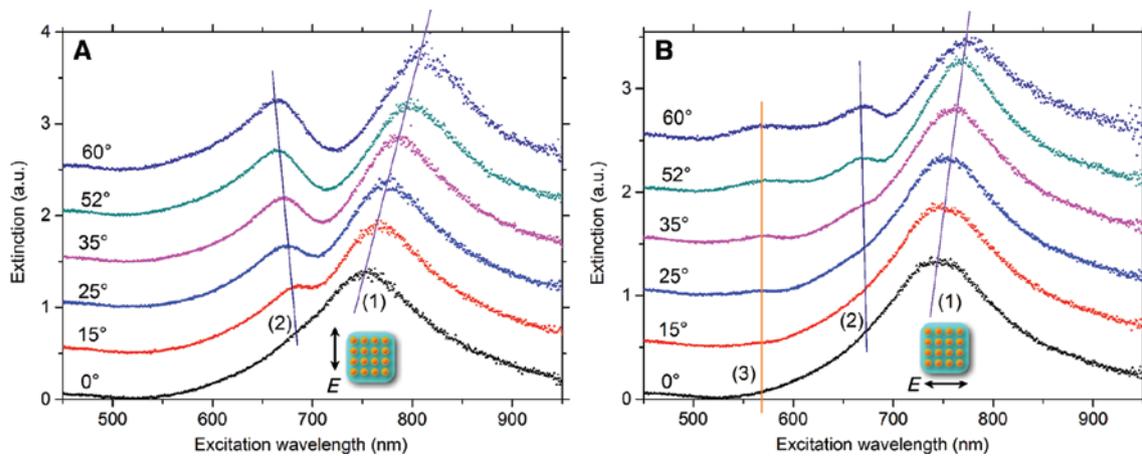

Figure 4: Extinction measurements resolved in angle in TE polarization (A). At normal incidence, only the dipolar mode [$\lambda \sim 740$ nm, (1)] is excited while, by increasing the incidence angle, the quadrupolar mode [$\lambda_Q \sim 680$ nm, (2)] is excited. At normal incidence, in TM polarization (B), only the dipolar mode (1) is also excited. When the incidence angle increases beyond 35°, the quadrupolar mode (2) and the vertical mode (3) are excited.

Indeed, for the range of wavelengths in the close vicinity of this plasmon peak, no radiative diffracted orders but evanescent waves [expressed as in Eq. (4)] are created by the grating structure. Being confined within the grating (decaying along z), the evanescent field associated to such waves can enhance the local plasmon fields, already excited by the impinging radiation, determining a CR of the dipolar modes of the single particles. In other words, the presence of evanescent and exciting fields, acting together on neighboring particles, induces a plasmonic coupling between them, which results in a decrease in their interaction energy and thus to a red-shift of the CR peak wavelength. It is not obvious though why this red-shift is proportional to the angle. By considering more closely the expression for β in Eq. (5), we can provide an intuitive interpretation of this observation. Actually, the amplitude $k_0\beta$, and hence the penetration depth of

the evanescent field into the nano-cylinders grating, is directly related to this angle. By plotting $k_0\beta$ for $m=\pm1$ (Figure 5A), we can observe that in one case ($m=+1$), the evanescent field is much less confined than in the other one ($m=-1$). The plot also shows that the amplitude of the electric field of this evanescent order is proportional to the incidence angle. As such, we can suppose that it is somehow contributing to the observed red-shift. Still, being the amount of evanescent orders propagating in the substrate quite large, we need to evaluate what is their overall effect. For this reason, numerical simulations have been performed for calculating the electric field value, at the top of the nano-cylinders (50 nm), corresponding to most of the evanescent diffracted orders ($-15<m<15$, $-10<n<10$) involved in the CR excitation, while modifying θ_{inc}. Selected plots for TE polarized exciting light and diffraction into air are reported in Figure 5B–F. An animation
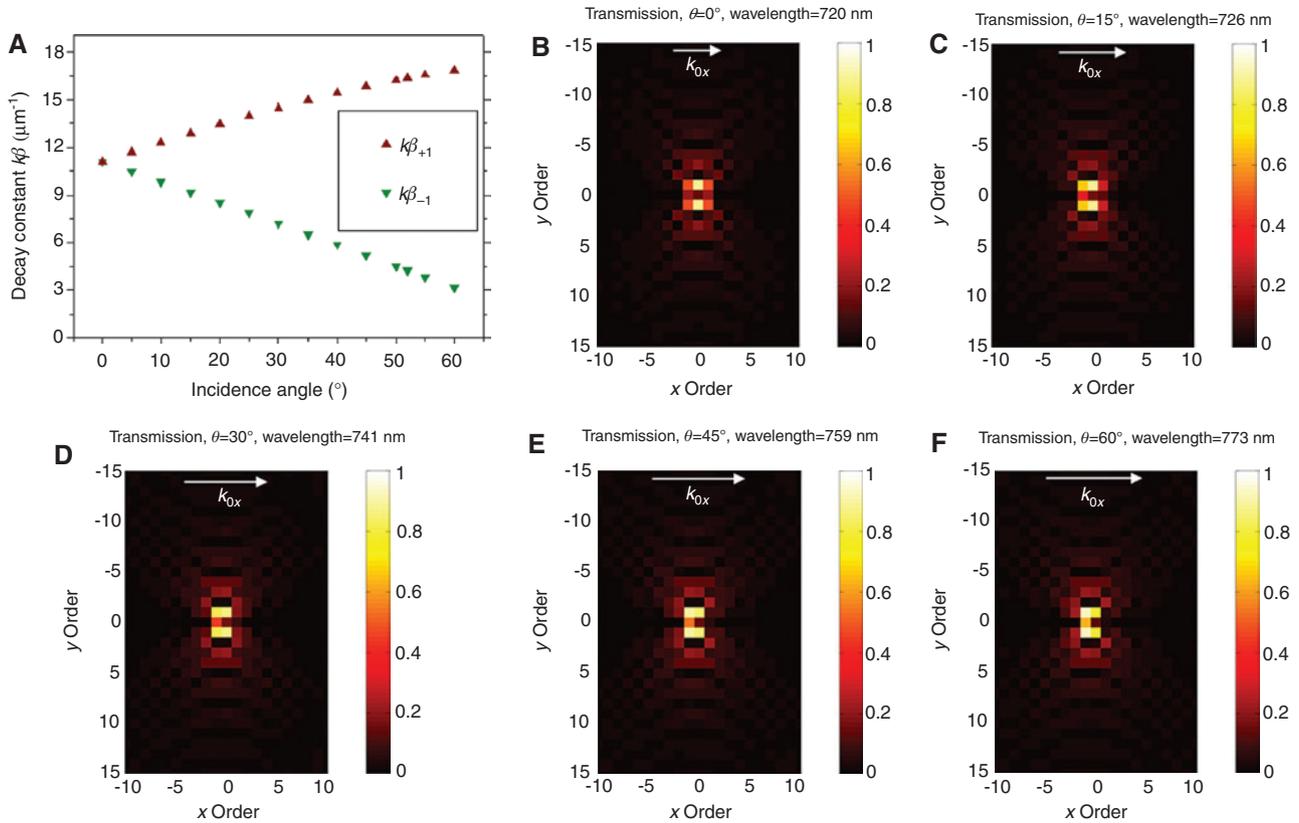
Figure 5: Interpretation of the spectral red-shift of the collective plasmon resonance observed while increasing the incidence excitation angle θ_{inc} as related to the presence of diffracted evanescent fields in the substrate. (A) Behavior of the decay constant $k_0\beta$ of the diffracted evanescent field ($m=\pm1$) as a function of θ_{inc}; (B)–(F) maps of the electric field amplitude, at a distance of 50 nm from the substrate, calculated for most of the evanescent diffracted orders involved in the CR excitation at different θ_{inc} values.

showing all the results for ($0° \leq \theta_{inc} \leq 75°$) with steps of 5° is instead available in the supplementary material.

A comparison of previous plots shows that the increase in the incidence angle corresponds to a progressive growth of the overall brightness of the map. This increase in the amplitude of the electric field implies that the total evanescent field in proximity of the nanocylinders is less and less confined for higher incidence angles and thus responsible of the red-shift of the CR. Noteworthy, it is exactly the presence of metal NPs in the (regular) array that is responsible for the significant increase in the overall electric field in the substrate. By simulating the same array (pitch and particle size), but in case of dielectric (TiO$_2$) nano-cylinders, it comes out (supplementary material) that the overall field in the substrate is, this time, almost negligible.

In Figure 4A, we can also observe another plasmon peak at lower wavelengths [$\lambda_Q \sim 680$ nm, (2) in Figure 4A] that appears at off-normal incidence. This mode can be identified as a quadrupolar one [27]; it grows in amplitude and seems to be slightly blue-shifted by increasing the

incidence angle: this behavior will be discussed later in the paper. Figure 4B shows the spectra obtained for the same incidence angle values and for a TM polarization of the exciting light. Also, this time, the dipolar mode only [(1) in Figure 4B] is obtained at normal incidence, and it has closely the same spectral position of that obtained with TE polarization; this is because the grating is a square with the same pitch in both directions. A red-shift of its spectral position also takes place even if less important than the one observed in the TE case. An interpretation of this red-shift can also be given by providing similar arguments as used before (Figure 5). However, it should be considered that, in case of TM polarization, the amplitude of the exciting field is strongly damped by a $\cos\theta_{inc}$ factor (Figure 3B). The smaller TM field amplitude is possibly responsible for both the more limited red-shift and the decrease in the collective plasmon mode amplitude for large incidence angles. In the TM polarization state, the quadrupolar mode starts appearing [at about the same spectral position, (2) in Figure 4B] at 35° incidence and with an amplitude that is more moderate than the TE case.

Both the appearance of the mode at larger angles and its smaller amplitude can be related to the $\cos\theta_{inc}$ damping factor of the exciting field amplitude.

More interestingly, a new mode, different from both dipolar and quadrupolar ones, can be noticed in the spectra at $\lambda\sim570$ nm [(3) in Figure 4B]. This peak is already visible at $\theta_{inc}=25°$ and can be attributed to a vertical mode corresponding to the plasmon oscillation along the height of the nano-cylinders. Indeed, it is reliable to consider that, in the TM mode only, the exciting field has a component $\sin\theta_{inc}$ that is exactly parallel to this direction and thus responsible for this excitation. Moreover, from the graphs, it is visible that the amplitude of this mode increases with the incidence angle, which matches well with the monotonously increasing behavior of $\sin\theta_{inc}$ in this angular interval. This argument suggests that the observed mode is exactly the vertical one. In our knowledge, this is the first time that this mode has been observed while performing this kind of measurement.

3 Theoretical simulations

A periodized version of Green's tensor formalism [30, 31] was exploited to simulate both transverse (TM) and longitudinal (TE) polarization extinction spectra as a function of the wavelength in the VIS-NIR range. Gold nano-cylinders were also considered (200 nm diameter and 50 nm height) spaced by 300 nm (center-to-center, both in x and y directions) and deposited on a semi-infinite glass substrate. A thin 70-nm-thick ITO layer was added on the silica underneath the particles. Behavior and spectral details observed through the numerical simulations match quite well the experimental results even if the characteristic plasmon modes generally show sharper features in the numerical curves than in the related experimental ones. There are at least two plausible mechanisms responsible for such differences. In one case, a plane-wave illumination has been assumed in the numerical simulations. This approximation is not true in the experimental case because of the high numerical aperture of both illumination (20×, 0.28 NA) and collection (50×, 0.42 NA) objectives. However, as detailed in the following, the choice of a plane-wave assumption was favored since it allowed unveiling a more complete scenario of the involved phenomena. On another side, even in case of an optimal fabrication procedure, discrepancies in the size and shape of particles are typical and they are usually not considered in the simulations. As an example, a characteristic defect of fabrication of nano-cylinders results in a conical shape. This can clearly influence the spectral shape of a vertical plasmon mode for which the vertical profile of the particle is important. Obtained curves are depicted in Figure 6A and B. Analogue simulations, but in case of single particle, were also performed and plotted in Figure 6C and D to be used as a reference. In Figure 6A and B, the normal-incidence, single-particle curve is plotted (dotted pattern) as a comparison with the array corresponding case. Figure 6E and F show instead selected curves of Figure 6A and B, respectively, in case of TM and TE polarization, for different angles of incidence (0°, 30°, and 60°), together with the corresponding distributions of the electric fields in proximity of the NPs, just above the substrate, in air. As numbered on the curves in Figure 6E and F, the various maps refer to specific spectral positions and the effect at the interface between substrate and NPs was considered for an incidence angle $\theta=60°$. These field maps are helpful for understanding the underlying physical phenomena taking place while the exciting light interacts with the array of NPs. When comparing the simulations (both TE and TM polarization) of the array of NPs with the ones related to the single NP, some distinctive features emerge. At normal incidence, the spectral position of the dipolar plasmon peak of the single particle ($\lambda_{LSP}\sim820$ nm; Figure 6C and D) is strongly red-shifted compared to the corresponding one in case of the array ($\lambda_{CR}\sim720$ nm; Figure 6A and B). Indeed, the presence of lobes oriented along the direction of the exciting field suggests the excitation of a dipolar term [field maps (1) in Figure 6E and F]. However, due to the presence of the grating (as discussed above), a coupling evidently takes place between the evanescent grating and plasmon modes that modifies the typical (single-particle) dipolar response into a collective dipolar resonance, blue-shifted if compared to the single particle resonance. It is also worth noting that the curves in Figure 6A and B confirm the pronounced red-shift of the CR with the angle of the incident planewave, already observed in experiments (Figure 4A and B) and qualitatively explained above; this red-shift is completely absent in the single-particle curves (Figure 6C and D): while changing the incidence angle, both the lineshape and spectral position of the dipolar peak remain the same (Figure 6C).

This is not true in the TM case (Figure 6D), where the increase in the incidence angle corresponds to a decrease in the dipolar curve amplitude. As observed above, this decrease can be attributed to the damping effect due to the decrease in the $\cos\theta_{inc}$ factor in the exciting field amplitude (Figure 3B). It could be speculated that the observed red-shift of the CR (in both TE and TM cases) is not real but is an apparent one due to the presence of the Rayleigh dip that can artificially move the broad peak to the red.
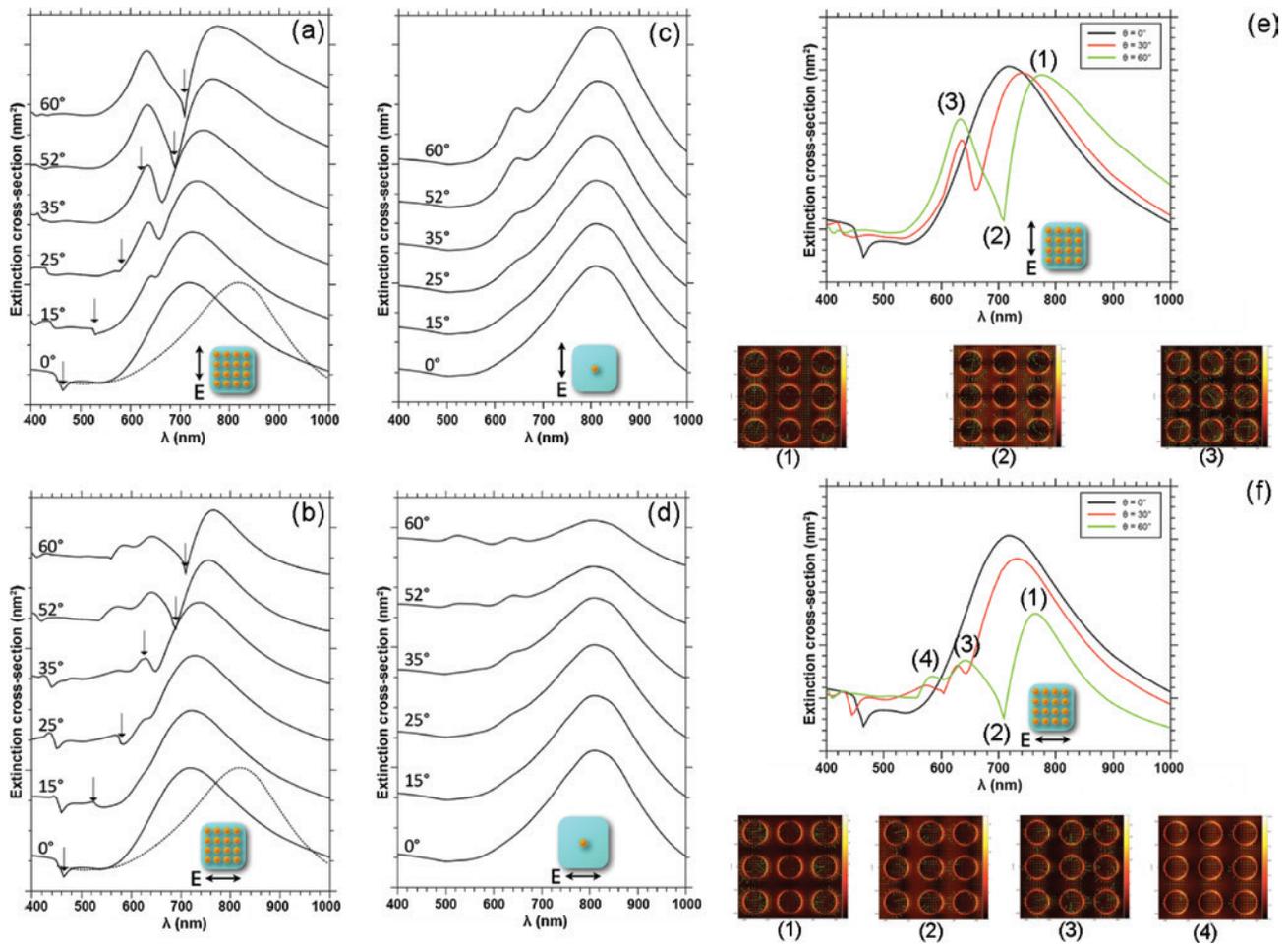
Figure 6: Numerical simulations of the extinction spectra as a function of the wavelength in the VIS-NIR range for different incidence angles of excitation. TE (A) and TM (B) excitation polarization in case of an array of nano-cylinders; TE (C) and TM (D) excitation polarization in case of a single nano-cylinder; description of resonance modes and their evolution for different incidence angles of excitation and corresponding field maps calculated at the bottom of the nano-cylinders in case of TE (E) and TM (F) excitation polarization.

This is to be excluded because at low incidence angles, where the Rayleigh dip is spectrally quite far from the CR position, the red-shift of the CR peak is already present and quite evident (for both TE and TM polarizations). If the damping of the CR peaks is taken into account, as again likely due to the approach of the Rayleigh dip, this concern should also be mitigated. Indeed, in the TE case, the observed damping is quite limited (Figure 6E). In the TM case (Figure 6F), it is more evident, but this is simply due to the fact that, again, by increasing the incidence angle, the $\cos\theta_{inc}$ factor in the exciting field amplitude (Figure 3B) is decreasing more and more due to geometrical reasons and the amplitude of the CR peaks decreases accordingly.

The increase in the angle of incidence of the exciting light is also related to the progressive excitation of a peak located at $\lambda\sim640$ nm in the single-particle simulations

(Figure 6C and D); by comparison with the experimental curves, we can attribute this peak to a quadrupolar mode, though it is slightly red-shifted in the experimental case ($\lambda_Q\sim680$ nm). The spectral position of this peak in the array simulations (Figure 6A and B) is the same, suggesting that the presence of the grating does not considerably contribute to the excitation of a collective quadrupolar mode as in the dipolar case. This is probably due to the fact that, in this spectral range, the (first) diffracted orders produced by the grating are all radiative, and thus, no evanescent coupling can take place. In both TE and TM field maps [(3) in Figure 6E and F], the shape and position of the bright four lobes, located around each NP, confirm the excitation of a quadrupolar mode. The lobes lay on the opposite sides of the NP, along the diagonals of the NP array (TE polarization) or along the array main axes (TM polarization). From simulations, new details also emerge

that could go unnoticed by considering only experimental data. In particular, the presence of a sharp dip spectrally located between the quadrupolar and the dipolar modes ($\lambda \sim 710$ nm), which is more visible for $\theta_{inc} > 25°$, is noteworthy. As indicated by black arrows in Figure 6A and B, this dip is exactly located at the Rayleigh wavelength λ_{RA} and corresponds to the crossing of the reflected grating order (1, 0) from the evanescent to the radiative propagation (in the substrate). It is interesting to notice that, exactly at the Rayleigh wavelength and for a 60° incidence, the incident wave propagates through the grating with minimum extinction. This can be attributed to the fact that evanescent orders do not carry energy. In this condition, it can happen that the coupling between these evanescent orders and the particles results in a local field nearly zero due to the fact that the particles are at the nodes of the stationary wave formed by the superposition of the incident field and the diffracted wave corresponding to Rayleigh wavelength: with no absorption inside particles, this results in the energy all carried in forward scattering (0th transmitted order) [32]. Further investigation will be devoted to the experimental verification of this possibility. Concerning the related field maps [position (2), Figure 6E and F], in the presence of this dip, the shape of the field

lobes suggests that the quadrupolar excitation dominates on the dipolar one. Last but not least, numerical simulations confirm the presence of the peak corresponding to the vertical mode [position (4) in Figure 6F]. The field map related to this mode, calculated for $\theta_{inc} = 60°$, shows a peculiar electric field distribution that cannot be attributed to a purely dipolar or quadrupolar mode. In order to obtain a better insight of the features of this mode, additional simulations have been performed, whose results are shown in Figure 7. Both 3D surface charges and field distributions around the single NP are reported for a TM excitation at 60° incidence (Figure 7A and B). In Figure 7C, the field map of the section of the single NP in the incidence plane is instead represented. Finally, in Figure 7D, the field map calculated at the vertical mode wavelength ($\lambda_V \sim 570$ nm) just beneath the interface (in ITO) is shown for each extinction curve of Figure 6B.

The symmetric and homogenous charge distributions on both the upper and lower borders of the NP (Figure 7A) represent a quite evident consequence of the vertical mode excitation ($E_y = E_{TM} \sin\theta_{inc}$; Figure 3B) induced by the TM wave. Quite interesting, though, is also the role played in the excitation by the transversal ($E_x = E_{TM} \cos\theta_{inc}$) component of the TM wave, which is more noticeable in Figure 7B
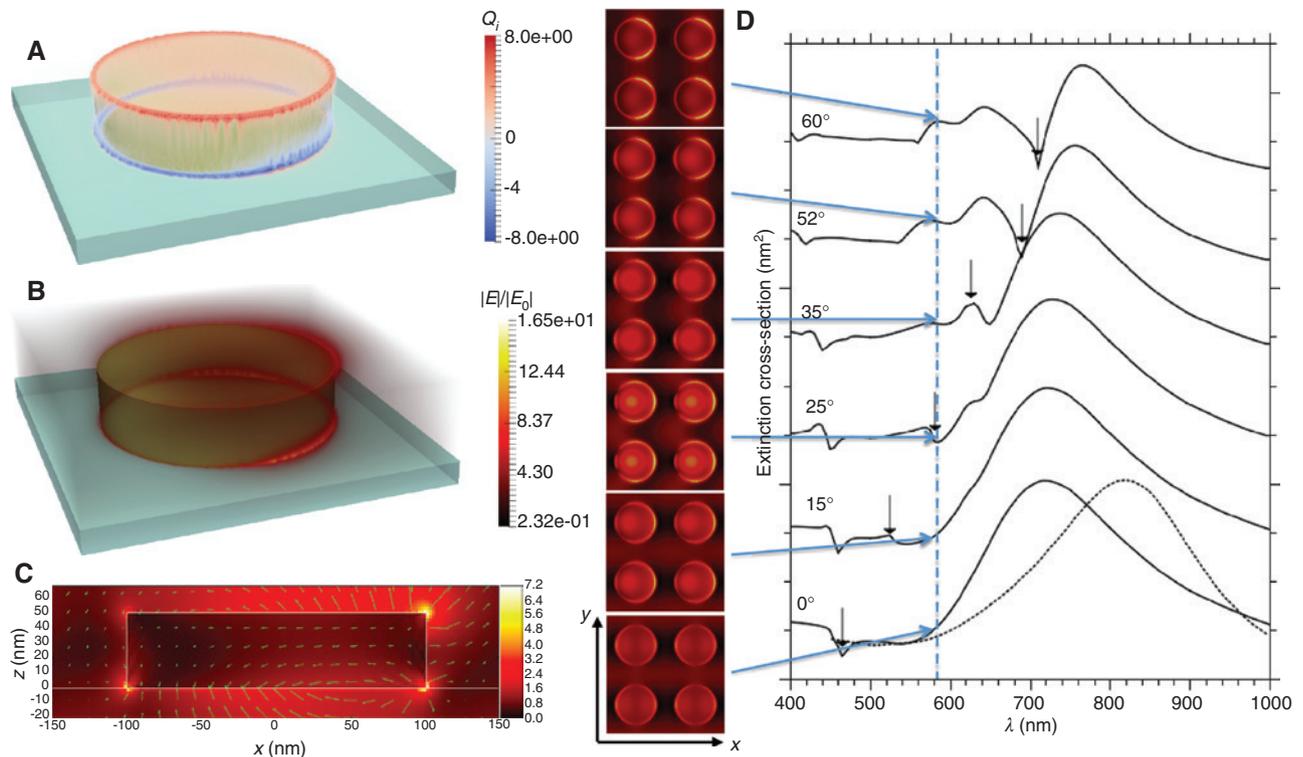

Figure 7: Numerical characterization of the vertical mode. 3D charge (A) and electric field (B) distributions around the single nanoparticle for a TM excitation at 60° incidence; field map of the section of the single nanoparticle in the incidence plane (C); evolution of the field maps related to the vertical mode ($\lambda_V \sim 570$ nm) calculated at the bottom of the nano-cylinders for different incidence angles of excitation.

and C. Indeed, the field asymmetry (Figure 7B) and the oblique field vectors on both upper and lower surfaces of the NP (Figure 7C) evidence that the plasmon excitation is to be considered as the result of the two field components of the TM wave. The field maps in Figure 7D also stress this hypothesis: the various bottom views show considerable field amplitudes both in the centers and on the borders of the NPs that can be respectively attributed to the effect of the horizontal and vertical components of the exciting TM wave. Moreover, depending on the excitation angle, the amplitude of the extinction peak ($\lambda_v \sim 570$ nm) evolves in adequation with the brightness of the related field map: an increase in the peak amplitude implies a brighter field map.

4 Conclusions

The plasmonic behavior of a 2D periodic array of Au nano-cylinders has been studied by performing angle-resolved extinction spectroscopy, in TE and TM polarization. The involved technique presents several advantages with respect to the standard (normal incidence) one. The pitch of the NP array has been chosen so that mainly evanescent diffracted orders were produced by the structure when excited with light whose spectral interval was in close proximity of the dipolar CR of the nano-cylinders. The excitation with increasing incident angles has put in evidence the collective plasmon resonance and its spectral red-shift, both due to a grating effect. An intuitive approach has been considered for relating the evanescent field, present in the sample substrate, with the resonance wavelength red-shift. Varying the excitation angle has also evidenced both a quadrupolar and a vertical plasmon mode. In particular, the latter can only be visible in TM polarization at off-normal excitation incidence.

References

[1] Kogelnik H. Coupled wave theory for thick hologram gratings. Bell Syst Tech J 1969;48:2909–47.

[2] Wood R XLII. On a remarkable case of uneven distribution of light in a diffraction grating spectrum. London Edinburgh Dublin Philos Mag J Sci 1902;4:396–402.

[3] Rayleigh L. On the dynamical theory of gratings. Proc R Soc London, Ser A 1907;79:399–416.

[4] Chartier G. Introduction to optics. New York: Springer-Verlag, 2005, pp. 328–9.

[5] Born M, Wolf E. Principles of optics. New York: Pergamon Press, 1980.

[6] Kanamori Y, Okochi M, Hane K. Fabrication of antireflection subwavelength gratings at the tips of optical fibers using UV nanoimprint lithography. Opt Express 2013;21:322–8.

[7] Yamada I, Ishihara T, Yanagisawa J. Reflective waveplate with subwavelength grating structure. Jpn J Appl Phys 2015;54:092203.

[8] Liu A, Fu F, Wang Y, Jiang B, Zheng W. Polarization-insensitive subwavelength grating reflector based on a semiconductor-insulator-metal structure. Opt Express 2012;20:14991–5000.

[9] Yu N, Capasso F. Flat optics with designer metasurfaces. Nat Mater 2014;13:139–50.

[10] Auguié B, Barnes WL. Collective resonances in gold nanoparticle arrays. Phys Rev Lett 2008;101:143902.

[11] Zou S, Janel N, Schatz GC. Silver nanoparticle array structures that produce remarkably narrow plasmon lineshapes. J Chem Phys 2004;120:10871–5.

[12] Zou S, Schatz GC. Narrow plasmonic/photonic extinction and scattering line shapes for one and two dimensional silver nanoparticle arrays. J Chem Phys 2004;121:12606–12.

[13] Markel VA. Divergence of dipole sums and the nature of non-Lorentzian exponentially narrow resonances in one-dimensional periodic arrays of nanospheres. J Phys B At Mol Opt Phys 2005;38:L115.

[14] Zou S, Schatz GC. Silver nanoparticle array structures that produce giant enhancements in electromagnetic fields. Chem Phys Lett 2005;403:62–7.

[15] Kravets V, Schedin F, Grigorenko A. Extremely narrow plasmon resonances based on diffraction coupling of localized plasmons in arrays of metallic nanoparticles. Phys Rev Lett 2008;101:087403.

[16] Chu Y, Schonbrun E, Yang T, Crozier KB. Experimental observation of narrow surface plasmon resonances in gold nanoparticle arrays. Appl Phys Lett 2008;93:181108.

[17] Vecchi G, Giannini V, Rivas JG. Surface modes in plasmonic crystals induced by diffractive coupling of nanoantennas. Phys Rev B 2009;80:201401.

[18] Vecchi G, Giannini V, Rivas JG. Shaping the fluorescent emission by lattice resonances in plasmonic crystals of nanoantennas. Phys Rev Lett 2009;102:146807.

[19] Kravets V, Schedin F, Kabashin A, Grigorenko A. Sensitivity of collective plasmon modes of gold nanoresonators to local environment. Opt Lett 2010;35:956–8.

[20] Giannini V, Vecchi G, Rivas JG. Lighting up multipolar surface plasmon polaritons by collective resonances in arrays of nanoantennas. Phys Rev Lett 2010;105:266801.

[21] Offermans P, Schaafsma MC, Rodriguez SR, Zhang Y, Crego-Calama M, Brongersma SH, Gómez Rivas J. Universal

scaling of the figure of merit of plasmonic sensors. ACS Nano 2011;5:5151–7.

[22] Zhou W, Odom TW. Tunable subradiant lattice plasmons by out-of-plane dipolar interactions. Nat Nanotechnol 2011;6:423–7.

[23] Nikitin AG, Nguyen T, Dallaporta H. Narrow plasmon resonances in diffractive arrays of gold nanoparticles in asymmetric environment: experimental studies. Appl Phys Lett 2013;102:221116.

[24] Luk'yanchuk B, Zheludev NI, Maier SA, Halas NJ, Nordlander P, Giessen H, Chong CT. The Fano resonance in plasmonic nanostructures and metamaterials. Nat Mater 2010;9:707–15.

[25] Salerno M, Krenn J, Hohenau A, Ditlbacher H, Schider G, Leitner A, Aussenegg F. The optical near-field of gold nanoparticle chains. Opt Commun 2005;248:543–9.

[26] Li H, Liu Q, Xie S, Zhou X, Xia H, Zhou R. Particle plasmons resonant characteristics in arrays of strongly coupled gold nanoparticles. Solid State Commun 2009;149:239–42.

[27] Meier M, Liao P, Wokaun A. Enhanced fields on rough surfaces: dipolar interactions among particles of sizes exceeding the Rayleigh limit. JOSA B 1985;2:931–49.

[28] Carron K, Lehmann H, Fluhr W, Meier M, Wokaun A. Resonances of two-dimensional particle gratings in surface-enhanced Raman scattering. JOSA B 1986;3:430–40.

[29] Félidj N, Laurent G, Aubard J, Lévi G, Hohenau A, Krenn JR, Aussenegg FR. Grating-induced plasmon mode in gold nanoparticle arrays. J Chem Phys 2005;123:221103.

[30] Paulus M, Gay-Balmaz P, Martin OJ. Accurate and efficient computation of the Green's tensor for stratified media. Phys Rev E 2000;62:5797.

[31] Chaumet PC, Rahmani A, Bryant GW. Generalization of the coupled dipole method to periodic structures. Phys Rev B 2003;67:165404.

[32] Biswas S, Duan J, Nepal D, Park K, Pachter R, Vaia RA. Plasmon-induced transparency in the visible region via self-assembled gold nanorod heterodimers. Nano Lett 2013;13:6287.